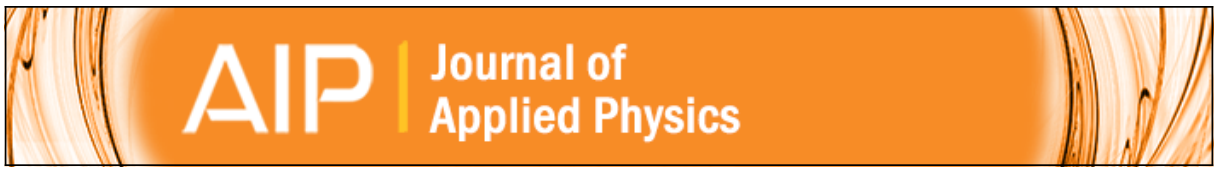

Determining the crystalline degree of silicon nanoclusters/SiO2 multilayers by Raman scattering

S. Hernández, J. López-Vidrier, L. López-Conesa, D. Hiller, S. Gutsch, J. Ibáñez, S. Estradé, F. Peiró, M. Zacharias, and B. Garrido

Citation: Journal of Applied Physics **115**, 203504 (2014); doi: 10.1063/1.4878175
View online: http://dx.doi.org/10.1063/1.4878175
View Table of Contents: http://scitation.aip.org/content/aip/journal/jap/115/20?ver=pdfcov
Published by the AIP Publishing

Determining the crystalline degree of silicon nanoclusters/SiO_2 multilayers by Raman scattering

S. Hernández,[1] J. López-Vidrier,[1] L. López-Conesa,[1] D. Hiller,[2] S. Gutsch,[2] J. Ibáñez,[3] S. Estradé,[1,4] F. Peiró,[1] M. Zacharias,[2] and B. Garrido[1]
[1]*MIND-IN2UB, Departament d'Electrònica, Universitat de Barcelona, Martí i Franquès 1, E-08028, Barcelona, Spain*
[2]*IMTEK, Faculty of Engineering, Albert-Ludwigs-University Freiburg, Georges-Köhler-Allee 103, D-79110, Freiburg, Germany*
[3]*Institute of Earth Sciences Jaume Almera, ICTJA-CSIC, Lluís Solé i Sabarís s/n, E-08028, Barcelona, Spain*
[4]*CCiT, Scientific and Technical Center, Universitat de Barcelona, Lluís Solé i Sabarís 1, E-08028 Barcelona, Spain*

(Received 7 April 2014; accepted 5 May 2014; published online 23 May 2014)

We use Raman scattering to investigate the size distribution, built-in strains and the crystalline degree of Si-nanoclusters (Si-nc) in high-quality Si-rich oxynitride/SiO_2 multilayered samples obtained by plasma enhanced chemical vapor deposition and subsequent annealing at 1150 °C. An initial structural characterization of the samples was performed by means of energy-filtered transmission electron microscopy (EFTEM) and X-ray diffraction (XRD) to obtain information about the cluster size and the presence of significant amounts of crystalline phase. The contributions to the Raman spectra from crystalline and amorphous Si were analyzed by using a phonon confinement model that includes the Si-nc size distribution, the influence of the matrix compressive stress on the clusters, and the presence of amorphous Si domains. Our lineshape analysis confirms the existence of silicon precipitates in crystalline state, in good agreement with XRD results, and provides also information about the presence of a large compressive stress over the Si-nc induced by the SiO_2 matrix. By using the Raman spectra from low temperature annealed samples (i.e., before the crystallization of the Si-nc), the relative scattering cross-section between crystalline and amorphous Si was evaluated as a function of the crystalline Si size. Taking into account this parameter and the integrated intensities for each phase as extracted from the Raman spectra, we were able to evaluate the degree of crystallization of the precipitated Si-nc. Our data suggest that all samples exhibit high crystalline fractions, with values up to 89% for the biggest Si-nc. The Raman study, supported by the EFTEM characterization, indicates that this system undergoes a practically abrupt phase separation, in which the precipitated Si-nanoclusters are formed by a crystalline inner part surrounded by a thin amorphous shell of approximately 1–2 atomic layers. © *2014 AIP Publishing LLC*. [http://dx.doi.org/10.1063/1.4878175]

I. INTRODUCTION

Controlling the size of silicon nanocrystals embedded in silicon oxides and/or silicon nitrides is a fundamental issue for the development of active optoelectronic materials with the desired electronic and optical properties.[1–3] Among the different existing techniques, the "silicon nanocrystal superlattice" approach, i.e., the deposition of alternated silicon-rich oxide (SRO) and stoichiometric silicon dioxide layers (SiO_2) that are subsequently annealed at high temperatures, has been shown to provide excellent control over the size of the precipitated Si nanoclusters (Si-nc).[4–6] During the post-deposition annealing process, a phase separation occurs driven by oxygen outdiffusion from the Si richest regions, that leads to the formation of Si-nc. This phase separation initially results in the precipitation of arbitrary structures that, at later stages of growth, produces the growth of amorphous clusters sphere-like in shape and limited in size by adjacent SiO_2 barriers. The crystallization of those clusters requires a large thermal budget that must be provided by annealing temperatures in excess of 1000 °C.[7] For sufficiently high thermal budgets, only a small region within the Si-nc/matrix interface remains amorphous due to high interfacial stress. The size of the amorphous and crystalline regions, as well as their relative amounts, strongly depends on both the deposition and subsequent annealing processes. Large thermal budgets are typically employed to obtain large, highly crystalline and interfacially relaxed Si-nc[7,8] with reduced non-radiative recombination paths, which are desirable for optoelectronic and photonic applications.

Some approaches have been used in the past for assessing the crystalline degree of the precipitated Si-nc, typically using transmission electron microscopy (TEM) techniques under different configurations.[8–10] Nevertheless, these approaches involve a long and difficult sample preparation that may also influence the structural properties of these systems. As an alternative to electron beam microscopies, non-destructive optical techniques have also been employed to monitor the precipitation process. However, these methods are not able to accurately provide reliable determinations of the crystalline degree of the Si-nc, and provide only rough estimations of it.[11–13] For instance, the intensity of the

photoluminescence (PL) emission has been proved to be directly related to the reduction of non-radiative paths (i.e., to lower amounts of defects), showing an emission enhancement for highly crystalline Si-nc.[11,12] Nevertheless, only a relative estimation of the crystallinity from sample to sample can be performed by PL measurements, as the emission strongly depends on the density of luminescent centers and the thickness of the probed region, but with no information from non-radiative recombination processes. Instead, Raman scattering is highly sensitive to both crystalline and amorphous phases of Si-nc. In fact, the amount of each phase in the Raman spectra can be expected to be proportional to the integrated intensities of the corresponding Raman bands. The different scattering cross-section of both phases and its dependence on the Si-nc size, however, make the evaluation of the crystalline degree of the Si-nc complex. Bustarret *et al.* determined the relative scattering cross-section of porous silicon as a function of the porous size,[14] which is useful for the calculation of the crystalline fraction. This approach has been widely employed in the literature for estimating the crystalline fraction in porous silicon and also in silicon nanocrystals (see for instance Refs. 15 and 16, respectively). However, it has recently been shown that this approach is highly inaccurate in the case of Si-nc.[13,17]

In this work, we use Raman scattering to evaluate the crystalline fraction of Si-nc in high-quality samples consisting of silicon-rich oxynitride/silicon dioxide ($SRON/SiO_2$) multilayers for different nominal SRON layer thickness. The Si-nc were initially characterized by means of energy-filtered transmission electron microscopy (EFTEM) and X-ray diffraction (XRD), revealing the presence of order arrangement of Si-nc with a notable crystalline phase. The Raman spectra for the Si-nc were modeled by considering phonon confinement effects and Gaussian-like functions for the crystalline and amorphous phases, respectively. In addition, using low temperature annealed (LTA) samples containing totally amorphous Si-nc, the relative scattering cross-section between the crystalline and amorphous phases was evaluated and modeled as a function of the crystalline Si domains. The determination of the relative cross sections allowed us to further evaluate the crystalline fraction of the precipitated Si-nc as a function of sizes. Our data and line-shape analysis suggest that all the samples annealed at high temperatures exhibit high crystalline fractions, thus confirming the good crystalline quality of the precipitated Si-nc.

II. EXPERIMENTAL DETAILS

$SRON/SiO_2$ multilayers have been deposited at 375 °C on fused silica substrates by means of plasma-enhanced chemical-vapor deposition (PECVD). In all samples, the thickness of the SiO_2 layers (t_{SiO2}) was kept constant at 2 nm, whereas the thickness of the SRON layers (t_{SRON}) was varied with nominal values of 2, 3, 4, and 5 nm. The total number of $SRON/SiO_2$ bilayers for all samples was 100, leading to a total nominal sample thickness of 400, 500, 600, and 700 nm (for SRON layer thicknesses of 2, 3, 4, and 5 nm, respectively). The stoichiometry of the silicon rich layers was $SiO_{0.93}N_{0.23}$, that produces a silicon excess of 17 at. % in the silicon-rich region. The precipitation of the silicon excess in the SRON layers was achieved by a post-deposition annealing process in a quartz tube furnace for 1 h under a N_2 atmosphere. Two identical sets of samples have been annealed at either 900 °C or 1150 °C, to produce amorphous and highly crystalline Si nanoclusters, respectively. Further details on the fabrication process can be found in Ref. 11. The absorption coefficient of low- and high-temperature annealed samples was determined by reflectance and transmittance measurements using the integrating sphere of a Bentham PVE300 photovoltaic spectral response system.

Prior to their study, the high temperature annealed (HTA) samples were cut in two pieces, one for performing TEM and another for XRD and Raman scattering measurements. In the case of TEM, samples were submitted to a mechanical polishing to a thickness below 20 μm followed by ion milling to electron transparency. EFTEM measurements were carried out in those samples using a JEOL 2010F TEM system operating at 200 keV and coupled to a Gatan Imaging Filter (with an energy resolution of 0.8 eV). The Si contrast was enhanced by energetically filtering the TEM image, selecting only the electrons with an energy loss within a window around the Si plasmon energy ($E_{Si} = 17$ eV). The size distribution of the precipitated Si-nanoclusters is, therefore, directly extracted from the analysis of the EFTEM images.

The crystalline ordering of the precipitated Si excess was monitored in the other pieces of the HTA samples by using XRD and Raman scattering techniques. In the case of XRD measurements, grazing-incidence X-ray diffraction (GIXRD) scans were acquired with a Panalytical X'Pert PRO MRD powder diffractometer equipped with a real-time multiple strip PIXcel detector. The measurements were performed with CuK_α radiation ($\lambda = 0.15406$ nm) by using a parallel beam geometry, with a constant angle of incidence of 0.3°. Rietveld full-pattern analyses were performed with the TOPAS 4.2 program (Bruker AXS, 2003–2009) in order to evaluate the lattice parameter and the size of the nanocrystals. For the analyses, the broad XRD band arising from the amorphous SiO_2 matrix was fitted with a split pseudo-Voigt (SPV) function, while a first-order polynomial function was used to fit the background signal.

Raman measurements were carried out using the 532-nm line from the second harmonic of a Nd^{3+}:YAG continuous laser. The Raman spectra were collected by an optical microscope from a Horiba Jobin-Yvon LabRam spectrometer, using an objective of ×100 magnification and analyzed by a highly sensitive CCD camera. The employed configuration provides a spatial resolution <1 μm that allows focusing the laser beam onto the $SRON/SiO_2$ films, once the samples are positioned under the objective in a cross-section configuration. In this way, an equivalent depth of SRON of about 2 μm is explored, achieving a strong signal enhancement from the Si-precipitates (and, in turn, reducing the relative signal from the fused silica substrate).

III. RESULTS AND DISCUSSION

A. Structural characterization

In Fig. 1, we display the EFTEM images of the HTA samples with different SRON layer thicknesses. As the

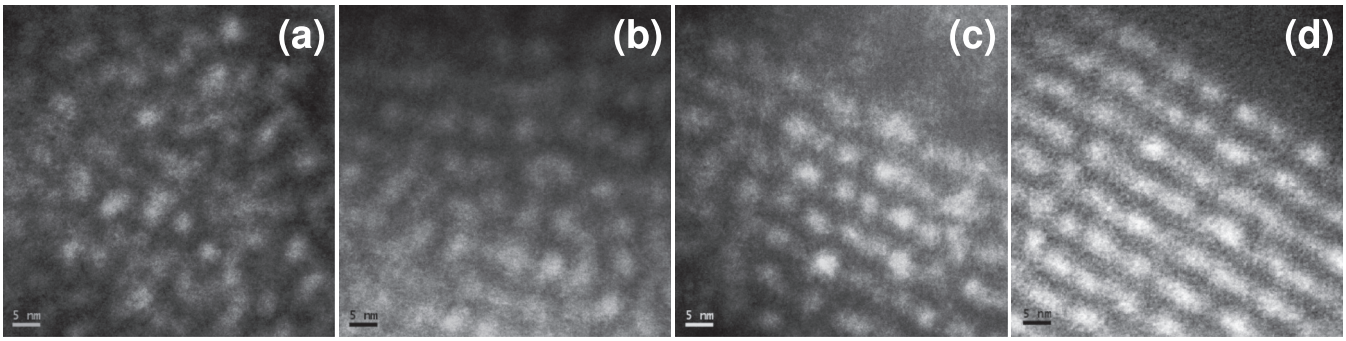

FIG. 1. Cross-section EFTEM images of samples with different nominal SRON thickness: (a) 2 nm, (b) 3 nm, (c) 4 nm, and (d) 5 nm.

transmitted electrons have been energetically filtered around the Si-plasmon, the bright contrast in the images corresponds to Si-precipitates, whereas the dark areas are associated with an environment of SiO_2. The images show two main features that are common for all four annealed samples: the precipitation of Si-nanoclusters and an increasing ordered arrangement of these Si structures at thicker t_{SRON}. It is important to mention here that the Si-nanoclusters are present only in the SRON layers that were intentionally deposited with a silicon excess. Therefore, the thickness of the SRON layers allows for controlling the final size of the aggregates, as previously reported.[18] On the other hand, the dark contrast of about 2 nm in thickness corresponds to the SiO_2 barrier layers, which is indicative that these regions maintain their stoichiometry even after the high temperature annealing[11] and, thus, the multilayered structure is conserved (transmitted electrons through dark areas present an energy loss of ~23 eV, which is typical from pure SiO_2).

Using the data shown in Fig. 1, together with some other images acquired in different regions along the samples, we have been able to determine the size diameter distribution of the Si-clusters for each of them. We have found that the size statistics follows a log-normal distribution with the form:

$$f(L_{0,clu}, \sigma_{clu}) \propto e^{-\left[\frac{(\ln L_{0,clu} - \ln L_{clu})^2}{2\sigma_{clu}^2}\right]}, \quad (1)$$

where L_{clu} and $L_{0,clu}$ correspond to the cluster size and mean cluster size, respectively, whereas σ_{clu} refers to the size dispersion in the log-normal distribution. The HTA sample with $t_{SRON} = 2$ nm shows a mean size of $L_{0,clu} = 2.4$ nm with a dispersion of $\sigma_{clu} = 0.11$. The fact that the Si clusters present a bigger size than the SRON layer thickness clearly indicates that some Si atoms have penetrated inside the SiO_2 barrier layers, making thinner and thicker SiO_2 and SRON layers, respectively, ($t_{SRON} \approx 2.4$ nm and $t_{SiO2} \approx 1.5$ nm). For the rest of the samples, we observed that the cluster size is slightly lower than the nominal thickness of the SRON layers and, thus, the final SiO_2 layer thickness between adjacent Si-nanocluster layers is slightly larger. Overall, the four samples display a narrow size distribution ($\sigma_{clu} \approx 0.1$), with a mean cluster size that scales with the nominal thickness of the SRON layers, displaying values of 2.4, 2.8, 3.3, and 4.1 nm, for $t_{SRON} = 2$, 3, 4, and 5 nm, respectively. In Table I, we have summarized the extracted data from EFTEM measurements.

XRD measurements have also been performed on the same HTA samples. Figure 2 shows a GIXRD scan from the sample with $t_{SRON} = 5$ nm. In addition to the broad and intense background signal arising from the SiO_2 substrate, centered just above 20° in 2θ, weak diffraction peaks corresponding to the (111), (022), and (311) reflections of Si are visible at around 28.6°, 47.5°, and 56.4°, respectively. Similar XRD scans were obtained for the rest of structures with the exception of the sample with $t_{SRON} = 2$ nm, which did not display any clear feature from Si-nc due to the strong contribution from the SiO_2 matrix.

Rietveld analyses allowed us to evaluate the lattice parameter (a_{XRD}) and the X-ray coherence length (L_{XRD}) of the nanocrystals. The inset of Fig. 2 shows the results of the Rietveld fits for the samples with $t_{SRON} = 3$ and 5 nm. Note that, for scaling reasons, the XRD signal from the SiO_2 matrix, fitted with a pseudo-Voigt function, has been subtracted from the spectra. As can be seen in this figure, good

TABLE I. Size distribution of the Si-nanoclusters and their crystalline fraction in HTA samples as determined by either EFTEM, XRD or Raman measurements. The lattice parameter (a_{XRD}) was obtained from Rietveld full-pattern analyses of the XRD scans, from which the effective hydrostatic stress on the Si nanoclusters, P, was further evaluated.

	EFTEM		XRD			Raman		
Nominal SRON thickness (nm) t_{SRON}	Mean cluster size (nm), $L_{0,clu}$	log-Normal σ_{clu}	a_{XRD} (Å)	Crystalline size, L_{XRD} (nm)	P_{XRD} (GPa)	Mean crystalline diameter (nm), $L_{0,cry}$	Log-Normal σ_{cry}	P_{Raman} (GPa)
2	2.4	0.11	…	…	…	1.9	0.11	1.1
3	2.8	0.13	5.416	2.2	1.0	2.6	0.08	0.3
4	3.3	0.09	5.428	2.6	0.2	3.1	0.07	0.09
5	4.1	0.10	5.431	3.2	0.0	4.0	0.06	0

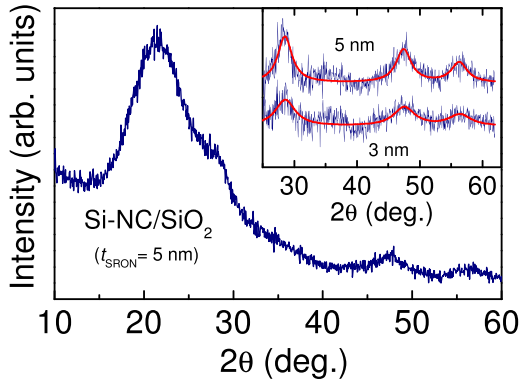

FIG. 2. Grazing-incidence X-ray diffraction scans of the SRON/SiO_2 multilayered sample with $t_{SRON} = 5$ nm. In the inset, the results of the Rietveld fits for the samples with $t_{SRON} = 3$ nm and 5 nm are shown, together with the experimental XRD scans after subtracting the contribution from the SiO_2 substrate.

agreement between the experimental and the calculated scans was found.

In the middle columns of Table I, the nanocrystal size and the lattice parameter (a_{XRD}) obtained from the Rietveld analyses for the samples with $t_{SRON} = 3$, 4, and 5 nm, are shown. In spite of its relatively poor sensitivity in relation to other analytical techniques, the XRD results confirm that the lattice parameter of the Si-nc decreases with t_{SRON}. This observation may be associated to increased matrix-induced compression of the Si-nc when their size is reduced.[9] Using the bulk modulus of Si, $B_0 = 98$ GPa,[19] the effective hydrostatic stress on the Si-nc can be evaluated with the expression $P = -3B_0\Delta a_0/a_0$, where $a_0 = 5.431$ Å (Ref. 19) is the lattice parameter of bulk Si, and $\Delta a_0 = a_{XRD} - a_0$. As can be seen in the table, the XRD results suggest that effective pressures as large as $\sim$1.0 GPa are applied to the Si-nc with $t_{SRON} = 3$ nm.

The Rietveld analysis also allows obtaining a rough estimation of the crystalline size of the Si-nc from the X-ray coherence length (L_{XRD}). We find that L_{XRD} gets reduced with decreasing the nominal SRON thickness, t_{SRON}. The mean sizes thus obtained are slightly lower than the ones determined by EFTEM, which might be related to the fact that the Si-nc contain a sizable proportion of amorphous material.

B. Raman scattering of Si-nc

Raman scattering measurements were also performed using the same set of HTA samples in order to extract further information about the crystalline state and size distribution of the nanoprecipitates. In Fig. 3, we present the Raman spectra in the optical phonon range of Si for multilayered samples with different nominal t_{SRON}. Two main features can be observed in all the spectra: a broad band in the range from 400 to 500 cm^{-1} and one sharp peak at around $\approx$520 cm^{-1}, which are related to Si disorder-activated acoustical and optical modes and to the Si crystalline transversal–longitudinal optical (TO-LO) phonon, respectively.[7] Moreover, some contribution from SiO_2 (either coming from the substrate or from the matrix) is still present in our spectra, even after using a cross-section configuration to acquire them. Despite the fact that the Raman signal of SiO_2 exhibits a low relative intensity in comparison to the signal coming from our Si-nanoclusters, this contribution is still relevant for the sample with the thinnest SRON layers (its Raman spectrum is alike to the one from pure SiO_2, with the addition of weak amorphous and crystalline Si contributions).

The presence of a disorder mode band in all the spectra is an indicator of the amorphous state of some Si aggregates, while the Si TO-LO mode, which is also observed in all the samples, provides a direct evidence of the presence of Si-precipitation in crystalline state (in agreement with XRD analysis). Therefore, these two contributions (amorphous and crystalline) are originated in different arranges of Si atoms within the matrix (i.e., different phases) and can be analyzed independently.

1. Crystalline contribution

First of all, let us consider the Si-related crystalline contribution to the overall Raman signal. One can observe in Fig. 3 that the intensity of the TO-LO mode rapidly increases with the SRON thickness (i.e., with the size of the Si-precipitates), which may be directly associated with an increase of the scattering volume for larger Si-nc. Nevertheless, the position and lineshape of the TO-LO mode is modified from sample to sample, displaying a broadening at lower frequencies and a shift to higher frequencies as the SRON thickness is reduced. Actually, the asymmetric lineshape is a consequence of the confinement of phonons inside the crystalline structures with sizes of about some nanometers, whereas the shift to higher frequencies is an effect caused by a high compressive stress applied to the Si-nc by the SiO_2 matrix (an additional shift to lower frequencies of some cm^{-1} is also produced by phonon confinement effects).[7,13] By analyzing the lineshape and position of the crystalline mode, it is possible to extract information about the crystalline size of Si-nc and the stress field to which they are submitted.

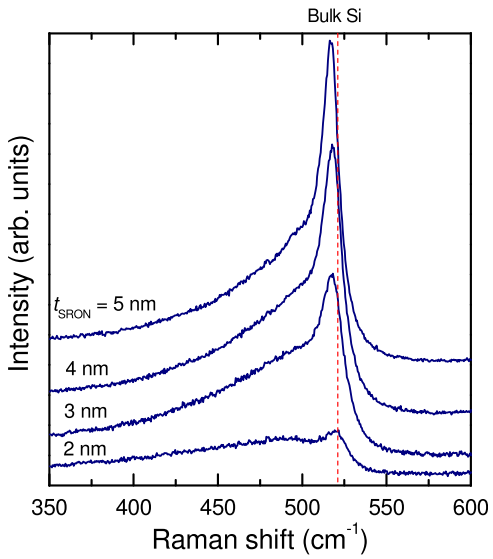

FIG. 3. Raman spectra of samples with different nominal SRON layer thickness of 2, 3, 4, and 5 nm, acquired under cross-section configuration. The vertical dashed line indicates the Raman shift corresponding to bulk crystalline silicon.

The Raman lineshape of the crystalline component of Si-nc under stress can be modeled using the phonon confinement theory modified by Crowe *et al.*,[13] assuming that the Si phonons are confined in hard spheres with a penetration into the surrounding SiO_2 matrix determined by their wavefunction decay [α, that is equal to 3 (Ref. 13)]. In this context, the Raman lineshape can be expressed as[7,13]

$$I(\omega,q,L,\alpha) \propto \int_0^1 \exp[-(2\pi qL/a)^2/(2\alpha^2)] \times [(\omega-\omega(q))^2+(\Gamma)^2]^{-1} q^2 \mathrm{d}q, \quad (2)$$

where ω is the Raman shift, Γ is the phonon damping, q is the reduced phonon wavevector, and L is the diameter of the crystalline domains. The phonon dispersion $\omega(q)$ is derived from the Brout sum rule to remove any anisotropy of the optical phonons in bulk silicon, modified to include a correction that accounts for the phonon pressure behavior[7,13]

$$\omega(q,P) = \sqrt{\omega_0(P)^2 - \frac{Aq^2}{q+0.53}}, \quad (3)$$

where A is to $1.261\times10^5\,\mathrm{cm}^{-2}$ and $\omega_0(P) = 521 + 4.9P(\mathrm{GPa})\ \mathrm{cm}^{-1}$ takes into account the pressure dependence of the zone-center TO-LO mode.[19] Introducing the possibility of having a log-normal size distribution also for crystalline domains, the total Raman lineshape can be expressed as a convolution of the contributions from the different sizes

$$I(\omega,q,L,L_{0,\mathrm{cry}},\sigma_{\mathrm{cry}},\alpha,P) \propto \int_0^\infty I(\omega,q,L,\alpha)\times f(L_{0,\mathrm{cry}}\ ,\sigma_{\mathrm{cry}})\mathrm{d}q, \quad (4)$$

with L, $L_{0,\mathrm{cry}}$, and σ_{cry} being the size distribution, mean crystalline size, and size dispersion, respectively, in the log-normal distribution of crystalline sizes.

Using this model we have fitted the crystalline part of the Raman spectra (from 490 to 560 cm^{-1}) of all samples by considering as free parameters the mean crystalline size $L_{0,\mathrm{cry}}$, the crystalline size dispersion σ_{cry} and the pressure P, including also a second-order polynomial function as a background to account for possible amorphous contributions. The initial guess of the fits for the effective pressure values applied by the SiO_2 matrix to the Si-nc has been taken from the XRD results. It is worth mentioning that the phonon damping coefficient (Γ) has been maintained constant at 10.5 cm^{-1} for all samples, as it has been found to be the value that better fits all the spectra. Actually, this value is much larger than the one we obtained for bulk silicon under the same experimental conditions, 3.5 cm^{-1}, which indicates reduced phonon lifetimes in the Si-nc.

In Fig. 4, we have plotted the resulting lineshape fits, in comparison to the experimental data. An excellent agreement between calculated and experimental curves is achieved for all samples, as can be observed in the figure. We have estimated the mean crystalline size from the fits, which show that the mean size $L_{0,\mathrm{cry}}$ increases with the

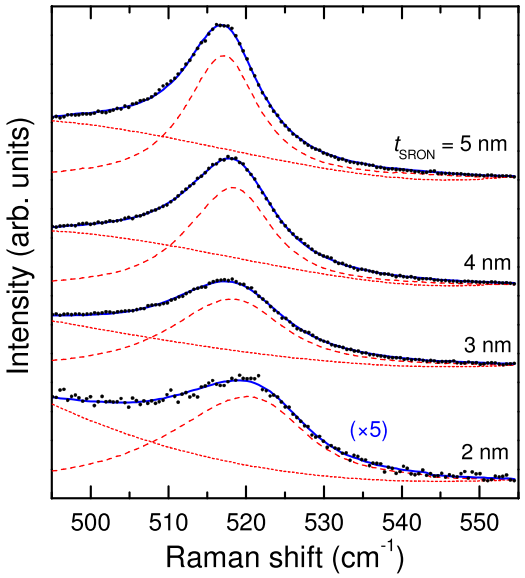

FIG. 4. Experimental Raman spectra of the crystalline part for samples with $t_{\mathrm{SRON}} = 2$, 3, 4, and 5 nm (black dots), compared to the obtained fits using the expression of phonon confined modes described in the text (blue solid-line). The short-dashed lines correspond to a polynomial background, whereas the long-dashed ones refer to the confined crystalline contribution.

SRON thickness: the values thus obtained are $L_{0,\mathrm{cry}} = 1.9$, 2.7, 3.1, and 4.0 nm (±0.2 nm) for $t_{\mathrm{SRON}} = 2$, 3, 4, and 5 nm, respectively. The log-normal size broadening σ_{cry} displays the opposite behavior, with narrower crystalline distributions for thicker SRON (see Table I). Moreover, the frequency shifts associated to hydrostatic compressive stress suggest reduced pressure values as the Si-nc size is increased (see Table I). The observed evolution with t_{SRON} is in good agreement with the XRD results. Nevertheless, the values obtained with the two techniques are somewhat different, which may be probably attributed to the fact that we have considered, as a first approximation, the properties of bulk Si (phonon pressure coefficient and bulk modulus) to model the compression of the Si-nc embedded in a matrix with much larger compressibility.[4,9,21] Experimental observations of compressive stress in matrix-embedded Si-nc have been reported by some authors by using XRD,[4] Raman scattering,[7,22] and also other experimental techniques such as photoluminescence[20,23] or high-resolution TEM.[24] Typical pressures for Si-nc embedded in SiO_2-based matrices are around some GPa or lower, which is in perfect agreement with the present results. In Table I, we have also summarized the values from crystalline size distribution and the pressures obtained with the Raman analysis.

Comparing the size values that were determined by EFTEM and Raman measurements, we find a slightly smaller size for the crystalline domains as obtained from the Raman analysis with respect to the total cluster size, with a difference of 0.12–0.14 nm for $t_{\mathrm{SRON}} = 3$, 4, and 5 nm, and slightly larger for $t_{\mathrm{SRON}} = 2$ nm ($\approx$0.5 nm). These data seem to suggest that the Si clusters are almost completely crystallized, exhibiting a thin amorphous layer in the interphase between Si and SiO_2. Nevertheless, a deeper analysis of the Raman data is required in order to properly determine the crystalline degree of the precipitated Si clusters.

2. Degree of crystallinity of the Si-nc

By analyzing the disorder band related to amorphous phases that appears in the range of optical modes (350–500 cm^{-1}, see Fig. 3), further information can be extracted from the Raman spectra. This contribution can be modeled by assuming that each branch of Si optical phonons from the first Brillouin zone contributes to the overall Raman signal due to the relaxation of $k \approx 0$ the selection rule, with a Gaussian-like lineshape.[25] In this way, and using the phonon dispersion curves of bulk Si, the Raman signal in the frequency range where our spectra were acquired (from 350 to 600 cm^{-1}) can be deconvoluted into three Gaussian-like contributions: one from disorder activated longitudinal acoustic modes (DALA) and two from optical modes (the disorder activated TO and LO modes, DATO and DALO, respectively). In Fig. 5, we present the Raman spectrum of a LTA SRON/SiO_2 sample that solely contains amorphous Si. The three contributions obtained for this sample, one acoustic and two optical (also shown in the figure), will be used below to take into account the Raman signal from amorphous Si.

It is worth noticing that the overall Raman intensity arising from amorphous Si aggregates is much larger than the equivalent one from crystalline systems, about one order of magnitude for the sample with $t_{SRON} = 5$ nm. In the inset of Fig. 5 we have depicted the Raman spectra, acquired under the same conditions, of this particular sample before and after HTA. Note that the higher intensity from the amorphous Si-clusters compared to the one from nanocrystalline Si evidences that the scattering cross-section is much larger for amorphous Si. Later, we will evaluate the scattering cross-section of both amorphous and crystalline Si in order to estimate, from the lineshape analysis of all the contributions that appear in the Raman spectra, the degree of crystallinity of Si-nc.

Thus, a deconvolution in the fitting routine of the Raman spectra of the SRON/SiO_2 multilayered samples has been performed by including the three Gaussian-like

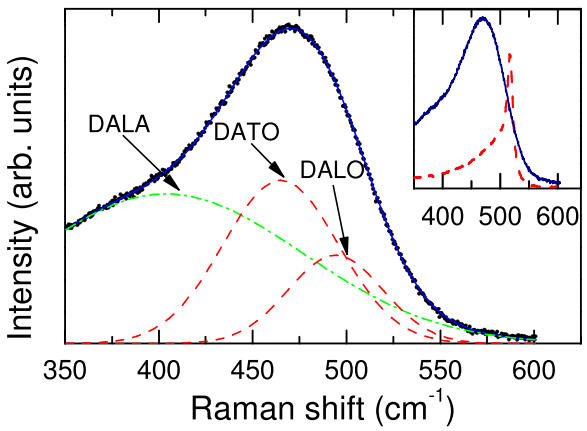

FIG. 5. Raman spectrum from amorphous Si of LTA sample with $t_{SRON} = 5$ nm (black dots), compared to the best fit (blue solid line) once deconvoluted into three different contributions, one acoustic (DATA, green dash-dotted line) and two optical (DATO and DALO, red dashed lines). In the inset, a comparison between the Raman spectra of the same sample before (blue solid line) and after (red dashed line) the annealing treatment at 1150 °C is displayed.

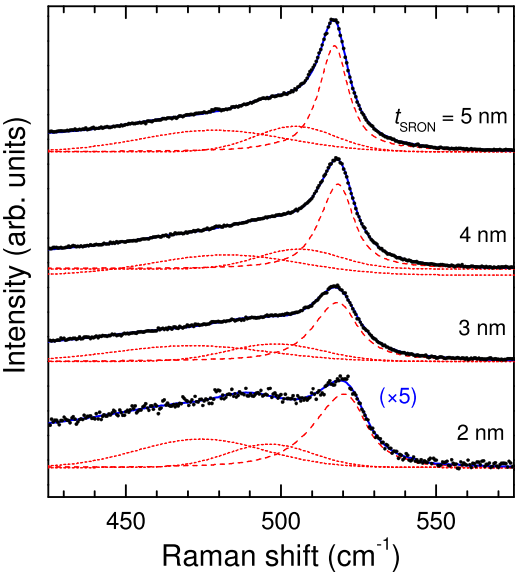

FIG. 6. Experimental Raman spectra in the range of Si optical phonons for samples with $t_{SRON} = 2$, 3, 4, and 5 nm (black dots), together with the best fits (blue full line) obtained by using the lineshape provided by the phonon-confined modes (red dashed line) and including Gaussian functions to account for the optical amorphous contributions (red short-dashed lines), as described in the text.

amorphous contributions and taking into account the previously determined crystalline contribution (see Fig. 6 and Secs. III B and III B I). The intensity factors of the three different amorphous contributions have been left as free parameters in the numerical calculation, whereas their position and their broadening have been taken from the deconvolution of amorphous Si (an interval within 5% of uncertainty was considered in the fitting procedure to account for possible distortions that may affect their lineshapes and positions). A small contribution from the SiO_2 matrix has also been taken into account by including the unpolarized Raman spectrum of SiO_2 with an intensity factor as a free parameter. Although the contribution from the matrix is very small, we found that the best accordance between calculated and experimental curves was achieved when this contribution was taken into account.

From the fits (see Fig. 6), using the data from the crystalline and amorphous contributions, we have evaluated the integrated intensity ratio, I_a^r, between the amorphous modes (i.e., the three disorder optical bands, with overall intensity equal to I_a) and that of the TO-LO band arising from crystalline Si (I_c): $I_a^r = I_a/I_c$. Following this procedure we extracted I_a^r values equal to 1.18, 1.15, 1.16, and 1.16 for $t_{SRON} = 2$, 3, 4, and 5 nm, respectively. These relative intensities can then be used to evaluate the crystalline fraction f_c of the system by using the relation[14]

$$f_c = \frac{1}{1 + \gamma I_a^r}, \tag{5}$$

which considers that the amount of each phase is proportional to its integrated intensity, once corrected for the different scattering cross-section. The factor γ is defined as the relative Raman cross-section of crystalline Si with respect to its amorphous phase and enters in Eq. (5) to include the

different Raman scattering efficiencies of both phases. In the case of bulk Si, it has been reported that the Raman cross-section of crystalline Si is one order of magnitude lower than in each amorphous phase (i.e., $\gamma = 0.1$),[14,26] which is in agreement to what is observed in the inset of Fig. 5 for $t_{SRON} = 5$ nm. This effect is due to the consequence of the scattering process of phonons with $k \neq 0$. In the case of Si-nc, the relative Raman cross-section strongly depends on the crystalline size, as first reported by Bustarret *et al.*[14] According to their work, the effect of crystalline size cannot be neglected to assess the total amount of phase transformed from amorphous to crystalline Si after the annealing process and, in turn, to evaluate the resulting crystalline fraction. For this reason, the relative cross-section γ for each sample was first determined from the Raman spectra of LTA and HTA samples by considering the amount of amorphous phase that is transformed into crystalline one. The integrated intensity of amorphous modes was measured in the same samples before the HTA treatment (i.e., in samples annealed at 900 °C to limit the growth process to only an amorphous state) and afterwards. The intensity of the amorphous contribution has been compared to the integrated intensity of the crystalline modes in the annealed samples, after subtraction of the reminiscent Si-amorphous contributions and correcting for absorption effects. Under these considerations, the relative cross-section γ can be calculated in terms of the expression

$$\gamma = \frac{\alpha^c\left(1 - e^{-2\alpha^c d_{light}}\right)}{I_a^{r,a}\alpha^a\left(1 - e^{-2\alpha^a d_{light}}\right) - I_a^{r,c}\alpha^c\left(1 - e^{-2\alpha^c d_{light}}\right)}, \quad (6)$$

where the relative scattering volumes are taken into account in terms of the absorption coefficients and the penetration depth imposed by the experimental set-up (d_{light}). In Eq. (6), $I_a^{r,a}$ and $I_a^{r,c}$ are the relative integrated intensities of the amorphous phases with respect to the crystalline ones as respectively obtained in LTA and HTA samples, whereas α^a and α^c are the corresponding absorption coefficients of each kind of samples (see Table II). The superscripts *a* and *c* refer to the samples annealed at low temperatures (amorphous Si) and after the HTA treatment (highly crystalline), respectively. In our measurements, it can be assumed that the light penetration d_{light} with the employed Raman configuration was limited to 2 μm, which is mainly determined by the width of the entrance slit of the spectrometer (at 100 μm) that works also as a pin-hole. It is worth mentioning that the absorption coefficients at the probed wavelength (532 nm) were experimentally determined in the studied samples (LTA and HTA ones) by using standard reflectance and transmittance measurements. We found values of the absorption coefficient that are in good agreement with the ones obtained in similar systems (see for instance Ref. 27).

No reliable amorphous signal coming from the LTA sample with $t_{SRON} = 2$ nm was obtained, as the Raman spectrum exhibits a strong background that masks the signal coming from amorphous Si-aggregates. For the rest of the samples, there is an increase of the relative scattering cross-section as the SRON layers get thinner (i.e., for smaller Si-nc), taking values of $\gamma = 0.178$, 0.135, and 0.104 for samples with $t_{SRON} = 3$, 4, and 5 nm, respectively (these results are summarized in Table II).

To obtain information about the dependence of γ on the crystalline size, we have fitted these experimental results to an exponential decay dependence $\gamma(L_{cry}) = \gamma(\infty) + [\gamma(0) - \gamma(\infty)] \times \exp\left[-\frac{L_{cry}}{L_{eff}}\right]$, equivalent to the one proposed by Bustarret *et al.*[14] Imposing that the relative scattering cross-section of very small crystalline domains is equal to that from amorphous aggregates [$\gamma(0) = 1$], and assuming that the one related to very large crystalline domains coincides with bulk Si [$\gamma(\infty) = 0.1$],[14,26] we can restrict the degrees of freedom to only one parameter, that corresponds to the exponential decay factor L_{eff}. In Fig. 7(a), we present the experimental data of γ as a function of the Si-crystalline size, together with the best fit of the exponential decay. An

TABLE II. Absorption coefficient and relative integrated intensities of the amorphous phases (with respect to the crystalline contribution) for amorphous and partially crystalline samples with different SRON thickness (columns 2–3 and 4–5, respectively). The relative scattering cross-section γ (column 6) was calculated from the previous data. The crystalline fraction of each annealed sample (last column) has been evaluated by considering the relative integrated intensity $I_a^{r,c}$ and the corresponding γ values.

t_{SRON} (nm)	α^a (cm^{-1})	α^c (cm^{-1})	$I_a^{r,a}$	$I_a^{r,c}$	γ	f_c (%)
2	6.9×10^2	5.2×10^2	…	1.16	0.235[a]	78
3	2.6×10^3	5.9×10^2	5.00	1.16	0.178	83
4	4.5×10^3	1.2×10^2	4.73	1.15	0.135	87
5	6.1×10^3	1.6×10^2	2.82	1.18	0.104	89

[a]Value extrapolated from the fitted curve. The rest of the γ values were determined from α^c, α^c, $I_a^{r,a}$, and $I_a^{r,c}$.

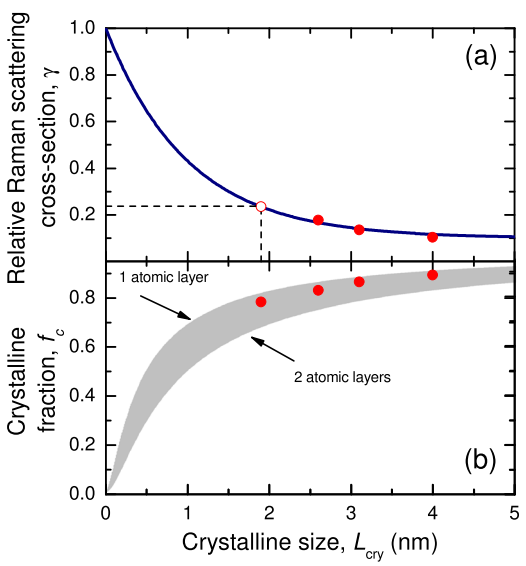

FIG. 7. (a) Relative Raman scattering cross-section γ of crystalline Si with respect to its amorphous phase as a function of the crystalline size. The red points are the experimental data, while the blue solid line corresponds to the function $\gamma(L_{cry}) = 0.1 + 0.9 \times \exp[-L_{cry}]$. The black dashed line indicates γ for the sample with thinner SRON layers ($L_{cry} = 1.9$ nm). (b) Calculated crystalline fraction for the annealed samples, using the I_a^r and γ values from Table II. The shaded region indicates the crystalline fraction of ideally spherical Si-nc with an amorphous shell between 1 (upper limit) and 2 atomic layers (lower limit).

exponential decay factor of $L_{eff} = 1$ nm perfectly reproduces our experimental data. The curve thus obtained allows us to estimate also the relative Raman cross-section for the sample with the smallest Si-crystalline domains [i.e., $\gamma(1.9\text{ nm}) = 0.235$]. This value has been included both in Table II and in the figure (dashed lines).

The determined relative Raman scattering cross-section γ turns out to have values close to that of bulk Si for crystalline sizes larger than $L_{cry} = 4$ nm (see also inset of Fig. 5), while it rapidly increases when the size of the crystalline domains is reduced. This behavior is in contradiction to that previously suggested by Bustarret *et al*. in porous Si,[14] where a decay function with a much longer decay factor of $L_{eff} = 25$ nm was obtained. The latter yields γ values very close to 1 for sizes of some nanometers in diameter (typical of Si-nanocrystals employed in electro-optical studies/applications),[3] overestimating the amorphous contribution in comparison to the crystalline one and, in turn, yielding also underestimated crystalline fractions (see below).[7]

Indeed, the relative Raman scattering cross-section γ already determined can be used to assess the crystalline fraction f_c by using Eq. (5) together with the relative amorphous integrated intensity I_a^r extracted from the Raman spectra of the annealed samples. In Fig. 7(b), we present the crystalline fraction as a function of the crystalline size for the four annealed samples with different SRON layer thickness. We find high crystalline fractions for all samples, which exhibit f_c values of 78%, 83%, 87%, and 89% for samples with $t_{SRON} = 2$, 3, 4, and 5 nm, respectively. Thus, it is concluded that f_c increases with t_{SRON}. Considering that our Si-nc are formed by a crystalline core surrounded by an amorphous shell (core-shell model[10]), the crystalline fraction can provide a direct relation between the crystalline size and the total cluster size, i.e., $f_c = \left(\frac{L_{0,cry}}{L_{0,clu}}\right)^3$. Using these assumptions and the mean crystalline sizes as extracted from the Raman band arising from crystalline Si, we have estimated the total cluster size. The values thus extracted are equal to 2.1, 2.8, 3.3, and 4.2 nm for $t_{SRON} = 2$, 3, 4, and 5 nm, respectively. These values are in excellent accordance to our experimental EFTEM data (see Table I, where L_{clu} values of 2.4, 2.8, 3.3, and 4.1 nm are reported in column 2), which suggests that the employed method provides a reliable evaluation of the crystalline fraction in Si-nc. The sample with the smallest Si-nc shows the largest deviation between both experimental techniques, probably due to the larger uncertainty associated with the small crystalline domains in this sample.

Together with the experimental data from the four samples, we plotted in Fig. 7(b) the crystalline fraction obtained for ideally spherical Si-nc composed by a crystalline core surrounded by an amorphous shell between 1 and 2 Si atomic layers (highlighted in grey).[19] As can be seen in the figure, all our values lie within this region, suggesting that the transition between nanocrystalline silicon and the SiO_2 matrix is practically abrupt. These results are in apparent contradiction with the estimated transition shell thickness reported by Daldosso *et al*.,[28] of about 1 nm. However, their samples consisted of a 200-nm Si-rich oxide, which may not constrain the Si atoms diffusion towards the surrounding SiO_2 matrix, thus forming a thicker amorphous region. Moreover, their theoretical model consisted of a relaxed structure, without considering the influence of the matrix stress exerted on the Si-nc. Actually, the presence of a very thin amorphous shell that surrounds the crystalline core is in perfect agreement with the conclusions of Ref. 9, where the transition shell was found to strongly depend on the Gibbs free energy, which, in turn, is highly influenced by the interfacial stress. Besides, in that work the interfacial stress over the nanoclusters was found to exponentially decrease when the crystalline size was increased, giving rise to a reduction of the thickness of the amorphous transition shell. This result, in agreement with our XRD and Raman results, implies increased crystalline fractions in crystalline Si-nc of increased sizes.

Overall, the results presented in this work confirm the good crystalline quality of Si-nc prepared with the multilayer approach, and also firmly support the non-destructive evaluation by the Raman-scattering technique of the structural properties of Si-nc based materials.

IV. CONCLUSIONS

Multilayers consisting of alternated SRON and stoichiometric silicon oxide layers were deposited on fused silica substrates by means of PECVD, varying the thickness of the SRON layers from 2 to 5 nm. The precipitation and crystallization of the silicon excess from the SRON regions into Si-nc was achieved by a high temperature annealing. EFTEM measurements showed the good structural properties of the resulting nanostructures, with Si-nc sizes proportional to the nominal SRON layer thickness. In turn, XRD measurements confirm the crystalline state of the precipitated Si-nc, suggesting also that these precipitates are subject to a matrix-induced compressive stress. The Raman spectra performed in all the samples were analyzed by considering contributions from crystalline and amorphous phases, using a phonon confinement model and Gaussian-like functions, respectively. By using samples containing amorphous Si-nc, the relative scattering cross-section of amorphous and crystalline phases was evaluated. Finally, the crystalline fraction was determined from the integrated intensities of each phase and considering their relative scattering cross-section. We found crystalline fractions larger than 80% in most samples that scale with the NC size, which is compatible with an amorphous shell thickness between 1 and 2 atomic layers.

ACKNOWLEDGMENTS

The research leading to these results has received funding from the European Community's Seventh Framework Programme (FP7/2007–2013) under Grant Agreement No: 245977, under the project title NASCEnT. The present work was supported by the Spanish national project LEOMIS (TEC2012-38540-C02-01) and MAT2010-16116.

[1]P. Löper, D. Stüwe, M. Künle, M. Bivour, C. Reichel, R. Neubauer, M. Schnabel, M. Hermle, O. Eibl, S. Janz, M. Zacharias, and S. W. Glunz, Adv. Mater. **24**, 3124 (2012).
[2]S. Chan and P. M. Fauchet, Appl. Phys. Lett. **75**, 274 (1999).

[3]J. López-Vidrier, Y. Berencén, S. Hernández, O. Blázquez, S. Gutsch, J. Laube, D. Hiller, P. Löper, M. Schnabel, S. Janz, M. Zacharias, and B. Garrido, J. Appl. Phys. **114**, 163701 (2013).
[4]M. Zacharias, J. Bläsing, P. Veit, L. Tsybeskov, K. Hirschman, and P. M. Fauchet, Appl. Phys. Lett. **74**, 2614 (1999).
[5]J. Heitmann, R. Scholz, M. Schmidt, and M. Zacharias, J. Non-Cryst. Solids **299**, 1075 (2002).
[6]J. Heitmann, F. Müller, M. Zacharias, and U. Gösele, Adv. Mater. **17**, 795 (2005).
[7]S. Hernández, A. Martínez, P. Pellegrino, Y. Lebour, B. Garrido, E. Jordana, and J. M. Fedeli, J. Appl. Phys. **104**, 044304 (2008).
[8]S. Hernández, P. Miska, M. Grün, S. Estradé, F. Peiró, B. Garrido, M. Vergnat, and P. Pellegrino, J. Appl. Phys. **114**, 233101 (2013).
[9]M. Zacharias and P. Streitenberger, Phys. Rev. B **62**, 8391 (2000).
[10]F. Iacona, C. Bongiorno, C. Spinella, S. Boninelli, and F. Priolo, J. Appl. Phys. **95**, 3723 (2004).
[11]A. M. Hartel, D. Hiller, S. Gutsch, P. Löper, S. Estradé, F. Peiró, B. Garrido, and M. Zacharias, Thin Solid Films **520**, 121 (2011).
[12]N. Daldosso, G. Das, S. Larcheri, G. Mariotto, G. Dalba, L. Pavesi, A. Irrera, F. Priolo, F. Iacona, and F. Rocca, J. Appl. Phys. **101**, 113510 (2007).
[13]I. F. Crowe, M. P. Halsall, O. Hulko, A. P. Knights, R. M. Gwilliam, M. Wojdak, and A. J. Kenyon, J. Appl. Phys. **109**, 083534 (2011).
[14]E. Bustarret, M. A. Hachicha, and M. Brunel, Appl. Phys. Lett. **52**, 1675 (1988).
[15]H. Tanino, A. Kuprin, H. Deai, and N. Koshida, Phys. Rev. B **53**, 1937 (1996).
[16]I. Stenger, B. Gallas, L. Siozade, C.-C. Kao, S. Chenot, S. Fisson, G. Vuye, and J. Rivory J. Appl. Phys. **103**, 114303 (2008).
[17]Ch. Ossadnika, S. Vepřeka, and I. Gregora, Thin Solid Films **337**, 148 (1999).
[18]M. Zacharias, J. Heitmann, R. Scholz, U. Kahler, M. Schmidt, and J. Bläsing, Appl. Phys. Lett. **80**, 661 (2002).
[19]S. Adachi, *Properties of Group-IV, III-V and II-VI Semiconductors* (John Wiley & Sons Ltd., 2005).
[20]K. Kůsová, L. Ondič, E. Klimešova, K. Herynková, I. Pelant, S. Daniš, J. Valenta, M. Gallart, M. Ziegler, B. Hönerlage, and P. Gilliot, Appl. Phys. Lett. **101**, 143101 (2012).
[21]R. Guerra, E. Degoli, and S. Ossicini, Phys. Rev. B **80**, 155332 (2009).
[22]T. Arguirov, T. Mchedlidze, M. Kittler, R. Rölver, B. Berghoff, M. Först, and B. Spangenberg, Appl. Phys. Lett. **89**, 053111 (2006).
[23]R. Rölver, S. Bruninghoff, M. Först, B. Spangenberg, and H. Kurz, J. Vac. Sci. Technol. B **23**, 3214 (2005).
[24]H. Hofmeister and P. Ködderitzsch, Nanostruct. Mater. **12**, 203 (1999).
[25]S. Wei and M. Y. Chou, Phys. Rev. B **50**, 2221 (1994).
[26]M. H. Brodsky, M. Cardona, and J. J. Cuomo, Phys. Rev. B **16**, 3556 (1977).
[27]L. Khriachtchev, M. Räsänen, S. Novikov, and L. Pavesi, Appl. Phys. Lett. **85**, 1511 (2004).
[28]N. Daldosso, M. Luppi, S. Ossicini, E. Degoli, R. Magri, G. Dalba, P. Fornasini, R. Grisenti, F. Rocca, L. Pavesi, S. Boninelli, F. Priolo, C. Spinella, and F. Iacona, Phys. Rev. B **68**, 085327 (2003).